Novel CO_2-thermic Oxidation Process with Mg-based Intermetallic Compounds and its Application to Energy Storage Materials

Younghwan Cha[a], Jung-In Lee [b], Panpan Dong[a], Xiahui Zhang[a] and Min-Kyu Song [a,b]

[a]Materials Science and Engineering Program, Washington State University, Pullman, Washington 99164, United States
[b]School of Mechanical and Materials Engineering, Washington State University, Pullman, Washington 99164, United States

Corresponding author E-mail: minkyu.song@wsu.edu (M.-K. Song)

Abstract

As an alkaline earth metal, elemental Mg is well-known for its ability to get oxidized by oxygen containing substances such as SiO_2 and TiO_2. Even in intermetallic compounds, Mg is readily oxidized, for instance, by gaseous CO_2. In this research, a novel strategy for the oxidation of Mg-based intermetallic compounds using CO_2 as an oxidizing agent was realized via simple thermal treatment, called 'CO2-thermic Oxidation Process (CO-OP)'. Furthermore, as a value-added application, electrochemical properties of one of the reaction products (carbon-coated macroporous silicon) was evaluated. Considering the facile tunability of the chemical/physical properties of Mg-based intermetallics, we believe that this route can provide a simple and versatile platform for functional energy materials synthesis as well as CO_2 chemical utilization in an environment-friendly and sustainable way.

Introduction

The climate crisis has attracted increasing attention from all over the globe. [1, 2]. It is urgent to reduce CO_2 emission and to find a way to recycle it into highly valued materials. To date, a variety of methods have been reported to directly or indirectly exploit CO_2 for the reduction of emissions. Many researchers have focused on the conversion of CO_2 into more valuable forms that can be used in solar energy conversion systems [3-5], electrocatalytic hydrocarbon production for fuels, or other forms of carbon-related chemicals [6-8], and functional graphene-like carbon synthesis [9-11]. Recently, Yin et al. reported the photocatalytic CO_2 reduction in an aqueous environment using nanometer-sized copper (II) oxides as a co-catalyst [4]. Under ultraviolet radiation, the nanosized copper (II) oxide particles act as effective catalytic sites, in which electrons are extracted from water molecules and then excited onto the conduction energy level by the photon energy, which in turn is used to reduce CO_2 into carbon monoxide (CO). Dai et al. studied heterogeneous catalysts to use CO_2 for the generation of useful organic carbonates such as cyclic carbonates and dimethyl carbonate [8]. They employed a combination of metal oxides, such as magnesium oxide, alumina, calcium oxide, and zinc oxide, and evaluated the stability and reusability of the oxides over the course of the synthesis. However, most of the organic routes for CO_2 reduction have critical issues related to the production efficiency (or final yield); achieving high production yield by nanoengineering requires an extensive effort and is very time-consuming. There have been a few reports, however, that have proposed inorganic routes for the reduction of CO_2. Chakrabarti et al. adopted a widely known in-class demonstration – combustion of magnesium ribbon in a dry ice bowl – into a more controlled environment to obtain few-layer graphene [9]. By analyzing the samples by Raman spectroscopy and transmission electron spectroscopy (TEM), they were able to confirm the formation of 'few-layer graphene' from the direct reduction of CO_2 using elemental magnesium as an effective reductant. Their focus was on the synthesis of novel carbon materials using the pure elemental form of metal species, such as magnesium and/or zinc, which later act as a sacrificing template by forming oxides during the synthesis.

In this study, we developed a novel and generally applicable method, called CO_2-thermic Oxidation Process (CO-OP), for environmental friendly and sustainable CO_2 utilization strategy through a simple thermal treatment with Mg-based intermetallic compounds, which can be readily oxidized with gaseous CO_2 and

further exploited for energy material synthesis. As a model system, Mg_2Si was chosen and explored deeper in this study; preliminary results of other candidate systems, such as Mg_2Sn and Mg_2Cu were also presented. As one of the possible value-added implications, we demonstrated electrochemical properties of the reaction product; carbon-coated silicon with a macroporous structure. The in-situ synthesized Si/C composite showed a high initial coulombic efficiency (83%) and stable cycling/rate performance (87% capacity retention after 400 cycles at 0.2C rate). The strategy involves the solid-state reaction for the synthesis of Mg-based intermetallic compounds and successive CO-OP in a CO_2 flow environment.

Results and discussion

The overall CO-OP with Mg-based intermetallic compounds is schematically illustrated in Figure 1, using Mg_2Si as model system. In the first step, 2 g of elemental magnesium (Mg) and 1 g of Si metal powders were manually mixed (excess Mg rather than stoichiometric molar ratio – Mg/Si = 2.3 to ensure full conversion of Si to Mg_2Si) and then heat-treated at 600 °C for 10 h in an Ar environment to obtain the intermetallic phase. It is worth noting that this solid-state reaction also can be used to synthesize other intermetallic compounds, such as Mg_2Sn and Mg_2Cu [12-16]. During the second step, the as-prepared Mg_2Si powder was placed in a crucible and heat-treated under a CO_2 flow environment at 700 °C for 10 h, which then converted to a MgO/Si/C composite. To understand the proposed synthesis, thorough fundamental studies were undertaken; (1) thermodynamic data collection for both the first solid-state synthesis for intermetallics and the second CO-OP to determine whether they are thermodynamically feasible (refer supporting information for more details‡), and (2) in-situ high temperature X-ray diffraction (HT-XRD) analyses (Figure 2a) to understand the phase evolution and to investigate reaction parameters for CO-OP with Mg_2Si. The Gibbs free energies at various temperatures for the CO-OP with Mg_2Si were collected from available database (Figure S1‡), which showed thermodynamic spontaneity; $\Delta G_{rxn} = -519$ kJ/mol at 700 °C. Furthermore, the in-situ HT-XRD results indicated that a temperature of approximately 500 °C was needed to initiate the oxidation reaction; a decrease of the Mg_2Si peaks and the appearance of the MgO and Si peaks were evident at the temperature range (Figure 2b and c). It implies that at least 500 °C of heating is required to initiate the CO-OP with Mg_2Si, which then could be related to activation energy of the oxidation of Mg_2Si. We also investigated microstructural and morphological change with controlling temperature; 600, 650, 680, 700, 800 °C / the holding time; 50, 100, 200, 400, and 600 min, to investigate experimental parameters and further understand the conversion process (Figure S2‡ and S3‡). The temperature / holding time control studies showed that, with a fixed ramping rate, heating up to 700 °C and maintaining at this temperature for at least 400 min was required to fully convert Mg_2Si into the MgO/Si/C composite.. Based on the results, we have implemented 700 °C and 10 h holding as conservative experimental parameters to ensure the full conversion of the intermetallic compound during CO-OP. Recently, J. Ahn et al. reported thermal stability of Mg_2Si at different temperatures in inert environment; 710 °C and 860 °C. They noticed that very little thermal decomposition occurred at 710 °C but at 860 °C, most of the Mg_2Si thermally decomposed and converted to macroporous Si [17]. We also performed similar investigation in order to check thermal stability of Mg_2Si. Mg_2Si powder was place in Swagelok reactor and tightly sealed in Ar

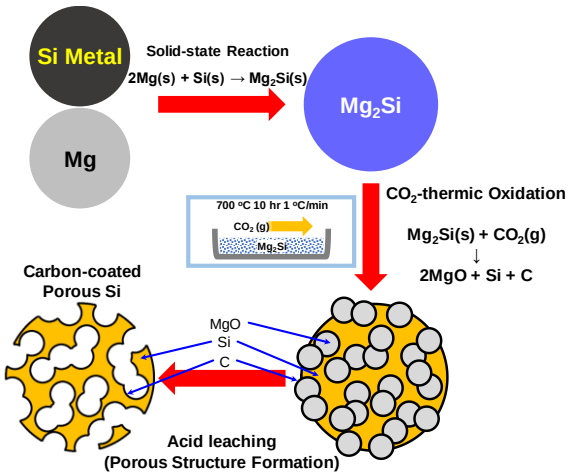

Figure 1. Schematic illustration for CO_2-thermic Oxidation Process (CO-OP) and carbon-coated porous silicon as an example of application for energy storage material.

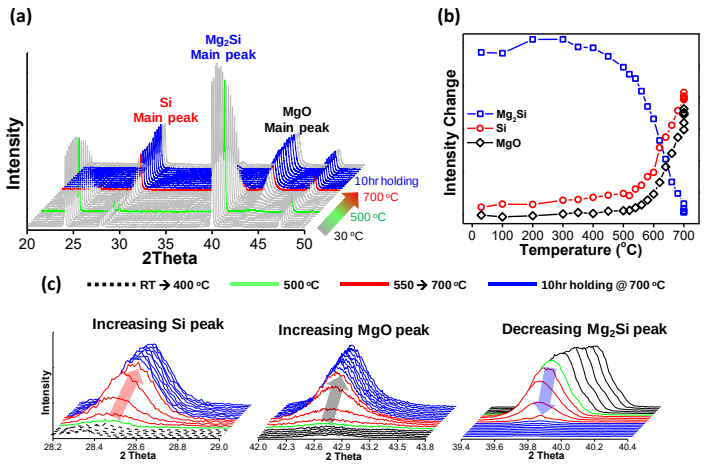

Figure 2. (a) in-situ high temperature XRD (HT-XRD) analysis of CO-OP with Mg_2Si, where phase evolution of MgO and Si as well as the decrease of Mg_2Si peak intensity can be clearly seen starting at around 500 °C (green lines). (b) Peak Intensity change during in-situ XRD showing clear phase evolution of Si and MgO. (c) Magnified in-situ HT-XRD peaks at around 2θ = 28~29°, 42 ~ 44°, and 39 ~ 40° where evident change in Si, MgO, and Mg_2Si peak intensities, respectively, can be seen with respect to temperature changes. It implies that at least 500 °C of heating is required to initiate/activate the CO-OP of Mg_2Si, which then might be related to activation energy of the oxidation reaction.

environment. Also, Ar gas was flown during the heating as well to prevent/minimize the introduction of unwanted impurity gases into the reactor, such as oxygen, that might exist and affect the reaction integrity despite of 99.9% purity of Ar gas used. As seen in Figure S4‡, sample heat-treated at 850 °C showed small amount of Si in ex-situ XRD and energy dispersive spectroscopy (EDS) analyses but sample heat-treated at 700 °C retained original Mg_2Si even after 10h holding. It is worth noting that the oxidation of pristine Si metal was tested under CO_2 environment (Figure S5‡). Typically, oxidation of Si in air or oxygen environment starts to occur at around 600~700 °C and gradually grows depending on temperature and time [18]. However, in this study, XRD pattern showed no distinct change under the given heating condition, indicating good stability of Si in CO_2 environment. Based on these facts, it can be inferred that the conservative heating parameters used in this study are sufficient for CO-OP while suppressing the thermal decomposition of Mg_2Si and oxidation of Si.

The change in the microstructure was investigated by ex-situ XRD and scanning electron microscopy (SEM). Figure 3a showed the XRD results at each step described in Figure 1, exhibiting clear phase transition from Mg_2Si → MgO+Si+C → Si+C and Figure 3b-e were the corresponding SEM images. The as-purchased Si metal powder (Figure 3b) exhibited smooth surface and wide range of particle size distribution (on average <15μm). Figure 3c showed drastic change in particle morphology after the intermetallic phase forming process. It is clearly seen that the solid-state reaction between Si and Mg brought about the change in overall particles size (<20 μm) as well as surficial features. These changes are because of the phase transition based on the reaction (i) below from Si with diamond cubic crystal structure (lattice parameter (a)=0.543 nm) to Mg_2Si with antifluorite structure (a=0.634 nm), which entails ~160% volume increase.

$$2Mg + Si \rightarrow Mg_2Si \qquad \text{(i)}$$

It is well-known that Mg is the main diffusive species during the solid-state reaction with Si. In general, the substance with a lower melting point has a relatively weaker atomic bonding and higher molar volume, which allows faster diffusion than the one with a higher melting point [13]; the melting points of Mg and Si are 650 °C and 1414 °C, respectively. Moreover, the nature of the chemical bonding in the Mg_2Si is known to be primarily covalent, with only approximately 8–9% ionicity between Mg^{2+} cation and Si^{4-} anion, which makes it even easier for Mg to diffuse into the innermost Si matrix, and hence enables the complete transformation to the intermetallic phase [14]. Subsequently, the as-prepared Mg_2Si powder was subject to CO_2 flow at 700 °C for 10 h, during which the thermal oxidation reaction of Mg_2Si occurred and resulted in a composite of MgO, Si, and C (Figure 3d) based on the reaction (ii) given below.

$$Mg_2Si + CO_2 \rightarrow 2MgO + Si + C \qquad \text{(ii)}$$

Despite that the XRD results clearly showed diminishment of Mg_2Si and development of MgO and Si, no conclusive evidence of the formation of crystalline carbon was observed. It might be attributed that the intensity of the MgO and Si peaks was too high to distinguish the small graphitic carbon peaks, or the carbon produced might be mainly amorphous. The morphology of the composite after the CO-OP was an

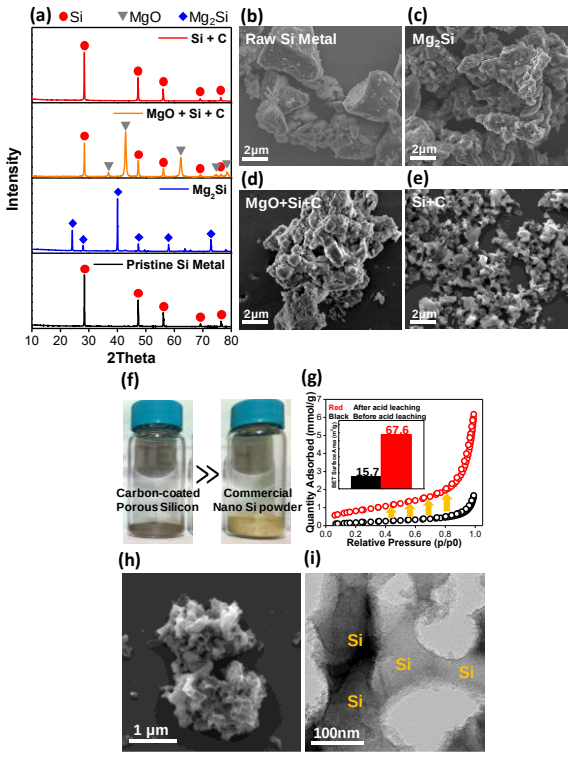

Figure 3. (a) ex-situ XRD analyses from starting Si Metal (black-bottom) to final Si/C composite (red-top), (b-e) Corresponding SEM images for each step. (f) Approximately 3 times higher tap density compared to commercial nano-Si powder. (g) N_2Sorption analysis before/after acid leaching showing increase in porosity and BET surface area (inset). (h) High magnification SEM image after acid leaching, which contains macro porous structure. (i) TEM image showing spherical macro pores and carbon layers on Si surface.

irregular-shaped lump with numerous speckles on the surface. This agrees well with the work of J. Liang et al., in which they performed air-oxidation of Mg_2Si and the surface morphology of the intermediate composite (MgO/Si) was fully covered with minute speckles [19]. In the last step, acid leaching was performed to furnish the porous structure by removing MgO, shown in Figure 3e. The removed oxides, such as MgO and possibly SiO_X, acted as sacrificial template for creating the macroporous structure which is believed to be one of the desirable features of Si-based anode materials; tapped density, which was measured by mechanically tapping a container until little further volume change is observed, is a critical factor in high energy applications and closely related to the size and porosity of the material. The Si/C composite (Figure 3f) exhibited almost 3 times higher tap density than the commercially available nanosized Si powder. N_2 adsorption–desorption analysis was performed (Figure 3g) to understand microstructural change during CO-OP. The results showed that the BET surface areas of samples before and after acid leaching were 15.1, and 67.6 m^2/g which proves the crucial role of MgO as a sacrificial template creating macroporous structure and relatively low surface area compared to typical nano-engineered Si-based anode materials [20]. Furthermore, the SEM and TEM high magnification images in Figure 3h and i showed that the Si/C composite after acid leaching exhibits porous structures with size >100 nm and uniform external layer of carbon.

Carbon coating is considered an essential part in the fabrication of the high energy Si anode material because the carbon layer can act as a physical buffer to volume change and, more importantly, help to form a sturdy solid-electrolyte interphase (SEI) layer leading to stable cycling performance [21-25]. Our strategy of the oxidation of Mg_2Si with CO_2can yield a carbon coating layer and a porous structured silicon simultaneously, whereas conventional routines for the fabrication of Si anodes require separate carbon coating step such as CVD [26, 27] or carbonization of the organic precursor [28-30], which is costly, time-consuming, and requires toxic chemicals. To prove the formation of carbon through CO-OP with Mg_2Si, TEM observations were first conducted to visually confirm the existence of a carbon layer on the Si surface. Figure 4a and b clearly shows a >20 nm thick, exterior layer, comprising a mixture of amorphous and graphitic carbon. To determine carbon content in the Si/C composite, thermogravimetric analysis was conducted in the temperature range from 25 °C to 700 °C (TGA, Figure 4b-inset). The weight loss is about 4.5% which is less than theoretical yield (30wt% based on the reaction (ii)). This discrepancy could be ascribed to the Boudouard reaction, $CO_2(g) + C \rightarrow CO(g)$, which explains chemical equilibrium of a disproportionation of carbon monoxide into carbon and carbon dioxide [31, 32]. Through this reaction, the incoming CO_2 gas can react with previously formed carbon into CO, which then exhausts out of the system. Even though the reaction is endothermic ($\Delta H = 172\ kJ/mol$ at 25 °C), at high temperature (typically > 700 °C), the free energy of the reaction dominated by entropic term ($T\Delta S$) becomes negative and proceeds spontaneously to produce CO [33]. As a matter of fact, recently many studies about catalytic effect of reactive alkali metal/metal oxide to promote the Boudouard reaction [3-5, 7, 31, 34-36]. During the CO_2 reduction in present study, one of the main reaction products is MgO which could accelerate the Boudouard process, resulting in the loss of

carbon. In addition, the oxidation of the intermetallic compound with gaseous CO_2 is an exothermic reaction (generating heat) which might be another factor that expedites the decrease in the carbon content. The EDS elemental mapping (Figure 4c) also confirmed that carbon was distributed uniformly in the particle. To obtain conclusive evidence and determine the nature of the carbon in the material, Raman spectroscopy (Figure 4d) was performed. Disordered and graphitic carbon peaks were evident at approximately 1330 /cm and 1580 /cm, respectively, which exhibited a 1:1 intensity ratio, which implies that the carbon synthesized through the CO-OP proposed in this study was a mixture of amorphous (or disordered) and graphitic carbon. Before acid leaching, there was a small peak shift for both the D and G peaks, probably owing to the existence of a strong MgO peak at approximately 1500 /cm. MgO in the sample might cause compressive stress to the carbon, which could result in the carbon peak shift [37].

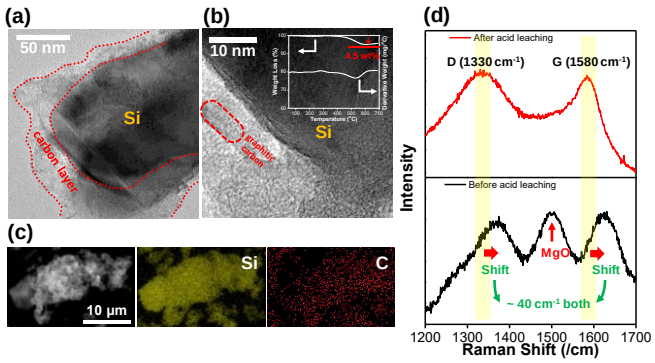

Figure 4. (a) TEM image showing >20 nm carbon layer (red dotted area) on Si matrix. (b) High magnification TEM image in which layered feature of graphitic carbon (red) is clearly seen. (c) EDS elemental mapping showing homogeneous distribution of carbon throughout the sample. (d) Raman spectroscopy before and after acid leaching showing that MgO is effectively removed from the system and it also provides decisive evidence on existence of carbon which implies the viability of the CO-OP of intermetallic compounds.

In order to investigate detailed internal structure of the Si/C composite, nano X-ray computed tomography was performed. Figure 5a was one of the X-ray scan images taken via high resolution absorption mode and clearly shows particles (about 7.5 μ in size) with well-connected porous structure inside. Also, in Figure 5b, a reconstructed cross-sectional view of the macroporous Si/C particle showed uniformly distributed pores (black) in the composite. It is more evident in the animated 3D reconstruction that majority of the pores in the composite particle are well-interconnected. It is highly recommended to check out 2D and 3D animattion video clips in Figure S6‡, where more comprehensive view of porous structure can be seen inside the composite particle.

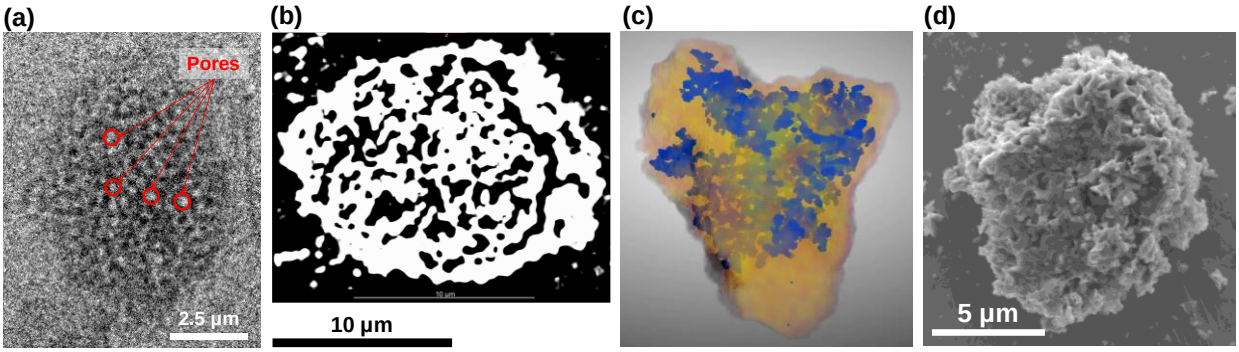

Figure 5. (a) One of the actual X-ray scan images of Si/C composite particle in high resolution mode, clearly revealing internal well-connected porous structure. (b) cross sectional image of reconstructed data, (c) Snapshot of 3D reconstruction of Si/C composite (yellow: Si/C and blue: pores); similar size Si/C particle, and (d) Si/C composite particle with similar size as the NanoCT result, which also exhibits macroporous structure. (refer ESI for more detailed 2D and 3D animations).

To understand the reaction mechanism between gaseous CO_2 and Mg_2Si, three diffusion mechanisms were proposed based on the behavior of gaseous CO_2 throughout the conversion, as shown in Figure 6; (1) CO_2(g) bulk diffusion, (2) surface diffusion, and (3) intra-/inter-particular diffusion. Initially, the CO_2 molecules move towards the Mg_2Si surface through the bulk gas layer. In our study, because the CO_2 gas flows continuously, the bulk diffusion should occur promptly. In sequence, the surface diffusion of the CO_2 molecules along the exterior of Mg_2Si particles occurs and the first oxidation reaction of Mg_2Si occurs,

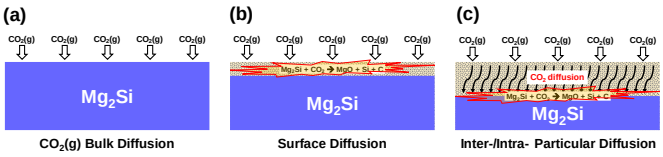

Figure 6. Hypothesized reaction kinetics between gaseous CO_2 and Mg_2Si. (a) initial bulk diffusion of gaseous CO_2, (b) surface diffusion causing early formation of MgO/Si/C composite, and (c) subsequent reaction between Mg_2Si and diffused CO_2.

which leads to the formation of the MgO + Si + C composite at the surface. Because the thermodynamic driving force for this oxidation reaction is sufficient ($\Delta G = -519$ kJ/mol at 700 °C), the surficial conversion might be finished at the very early stage of the process. According to the in-situ HT-XRD, this initial conversion would take place during heating to ca. 500 °C. After the formation of the first surficial composite layer, the consecutive supply of CO_2 gas molecules into the interior of the Mg_2Si should be achieved through inter-/intra-particular diffusion of the CO_2 molecules through the newly formed MgO + Si + C composite layer. Song et al. investigated gaseous CO_2 intake kinetics of a MgO matrix and found out that the intra-particular diffusion is the rate limiting factor among other diffusion mechanisms, such as surface (film) diffusion, inter-particular diffusion, and bulk diffusion [38]. The composite layer (MgO + Si + C) in the current study is more complicated than the work of Song et al., but it would be reasonable to propose that the gaseous CO_2 may diffuse through the composite layer initially formed on the surface of Mg_2Si and continuously promote the oxidation reaction with internal Mg_2Si until full conversion to the composite.

To further confirm the proposed concept in the present study, we also conducted same heat treatment with magnesium stannide (Mg_2Sn) and magnesium copper intermetallic alloy (Mg_2Cu). As seen in Figure S7‡ and S8‡, XRD results showed that Mg_2Sn and Mg_2Cu were successfully converted to corresponding composites by CO-OP. Particularly, in-situ HT-XRD investigation showed similar trend as Mg_2Si with increasing temperature; decrease in peak intensity of intermetallic compounds and increase in reaction products. We were not able to see Sn during the heating because the melting point of Sn is 232 °C, which later appeared during cooling (Figure S7b-inset). The unexpected formation of SnO_2 is still under investigation but it might be attributed to oxidative nature of Sn. It is well-known that Sn forms the oxide when exposed to an air/O_2. At elevated temperature, Sn could react with CO_2 and form the oxide.

As one of the applicative areas of the current study, the electrochemical properties of the final carbon-coated porous Si were evaluated. The typical procedures for the fabrication of highly functional Si/C composites for advanced lithium-ion batteries require a separate carbon coating step, which is one of the reasons that the commercialization and scale-up of Si anode technologies has been impeded. However, our CO-OP approach can afford a porous structured Si as well as carbon coating simultaneously through a one-step thermal treatment with CO_2 as source for the carbon. A typical CR2032-type coin cell configuration was used to test the cycling performance of the in-situ synthesized material (detailed description in the experimental section). As shown in Figure 7a, the initial lithiation and delithiation voltage profile showed typical crystalline-to-amorphous phase transition of a Si-based anode, in which the specific capacities were 2732 mAh/g and 2273 mAh/g, respectively, leading to a high initial coulombic efficiency of 83.2%. Furthermore, the carbon-coated porous silicon obtained from the proposed CO-OP showed a good rate capability (Figure 7b) of approximately 1000 mAh/g at a 1.0 C rate, which recovered back to 2000 mAh/g at 0.2 C rate. Representative lithiation/delithiation profiles at each C rate were shown in Figure 7c, indicating phase transition of amorphous Si during cycling. In Figure 7d and e, cycling performances at 0.2 C rate of the Si/C composite were compared with bulk Si and air-oxidized Si samples. They showed good cycling stability over 400 cycles exhibiting ~87% capacity retention. It is worth to note that the bulk Si was fabricated by bill milling of as-purchased Si metal, exhibiting comparable size with the Si/C composite in this study (Figure S9a‡). Figures S9b-d‡ show morphology and XRD result of Si sample via air-oxidation of Mg_2Si, where it showed similar particle size but with mesoporous (<50nm) structure. It is noteworthy that the role of MgO can be clearly seen in figure S9c‡ where less than 50nm sized pores were appeared after acid leaching.

The stable cycling performance of Si/C composite in this study might be attributed to the low surface area and carbon-coating layer on Si surface, minimizing consumption of electrolyte over cycling, forming sturdy SEI layer on the composite, and preventing pulverization of Si host by carbon layer acting as physical buffer.

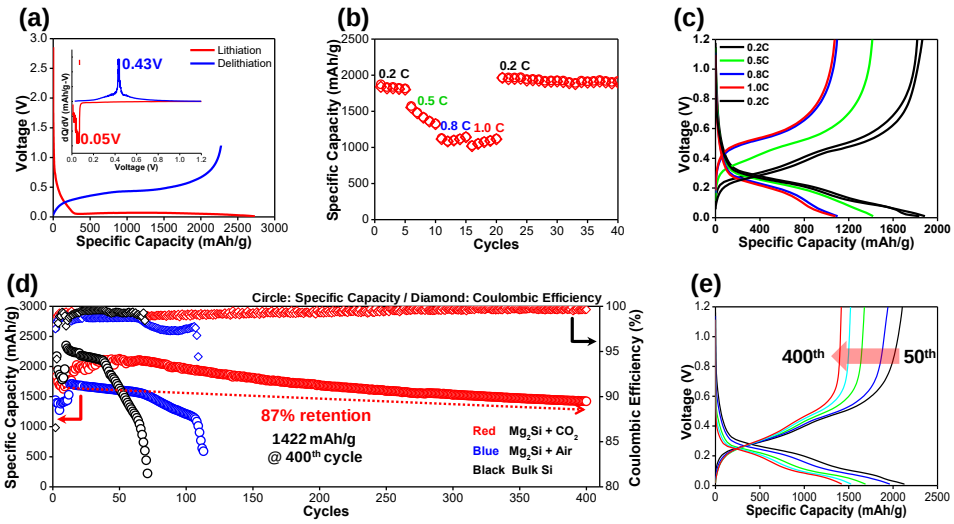

Figure 7. (a) First cycle voltage profile; lithiation and delithiation capacities are 2732 mAh/g and 2273 mAh/g, respectively, resulting in >83.2% coulombic efficiency (inset: dQ/dV plot for the first cycling showing sharp peaks at ~0.05V, indicating phase transition of crystalline Si to amorphous Si. (b) Rate capability result exhibiting ~1000 mAh/g specific capacity at 1.0 C-rate and recovering back to ~2000 mAh/g at 0.2 C-rate. Si/C composite from CO-OP of Mg_2Si (red) showed relatively better rate performance at fast current condition than Si from air-oxidation of Mg_2Si (blue). (c) Representative voltage profiles for each C-rate; 0.2C-black, 0.5C-green, 0.8C-blue, 1.0C-red, and 0.2C(recovery)-black). (d) Comparison of 0.2 C-rate cycling performance among bulk Si Metal, Si via air-oxidation of Mg_2Si, and carbon-coated porous Si from current study. (e) Lithiation-delithiation profiles of carbon-coated porous Si at different cycles.

The long-term cycling performances at 0.5 and 1.0 C-rate (1C=1st lithiation capacity) are also shown in Figure S10‡. Even though it showed gradual decrease over long term cycling, it still displayed 80% capacity retention after 559th and 478th cycle at 0.5 and 1.0 C rate, respectively, which could probably be improved further by optimizing the process.

Capacity recovery during the initial 50 cycles was commonly observed, which might be attributed to an increase in utilization of active materials over cycling. A modest decrease in the coulombic efficiency to 98.7% was observed during the early capacity recovery stage, but it was gradually recovered. After the recovery period, specific capacity was slowly fading but no sudden death, which is typically due to the consumption of electrolyte, was observed. Since the particles size of active material was still in the micrometer scale, gradual degradation resulting in capacity fading might not be fully suppressed, but the degree of capacity fading was not too severe and reached 400, 900, and 1000 cycles maintaining 1422, 1028, and 987 mAh/g of specific capacity, at 0.2, 0.5, and 1.0 C rate respectably, with more than 99.9% coulombic efficiency.

Conclusions

In conclusion, a novel CO_2-thermic Oxidation Process (CO-OP) has been demonstrated using Mg-based intermetallic compounds. Thorough investigation on the proposed approach with Mg_2Si as a model system was performed, including a thermodynamics feasibility study, an in-situ phase evolution analysis, and intensive microstructural characterization of the CO_2-thermic oxidation reaction. The proposed route was found to be an effective way to fabricate promising anode material for advanced energy storage systems. The reaction product showed excellent long-term cycling stability and moderate rate capability. These results show that the proposed CO-OP with oxidative intermetallic compounds is a promising pathway for recycling and utilizing CO_2 gas as feedstock for the formation of functional energy materials. We anticipate that the present study can provide not only a green alternative approach for current CO_2 reduction research but also a novel platform for the design and fabrication of high energy density materials development.

Experimental

Synthesis of Mg_2Si

1 g of commercially available silicon metal powder (~15 μm, Panadyne Inc.) and 2 g of magnesium powder (~325 mesh, Alfa Aesar) were manually mixed (the amount of magnesium was slightly higher than the stoichiometry (Mg/Si = 2.3:1) of Mg_2Si to guarantee the full conversion of silicon to silicide) and then

placed into a stainless-steel Swagelok reactor. The reactor was tightly sealed in an argon-filled glove bag to minimize the exposure to the air; it was purged at least three times with high purity argon gas prior to sealing. Immediately after the sealing, the autoclave reactor was placed in a tube furnace (MTI corp.), heated at a ramping rate of 1 ^{o}C/min up to 500 ^{o}C, and held for 10 h before cooling down to room temperature. The as-prepared magnesium silicide powder was kept in a vial for later use.

CO_2-thermic Oxidation Process with Mg_2Si

Approximately 2 g of as-prepared Mg_2Si powder was manually grounded and spread in an alumina crucible. The crucible was then placed in a tube furnace, which was heated at a ramp rate of 1 ^{o}C/min and maintained at 700 ^{o}C for 10 h under a carbon dioxide (99.9% purity) gas flow. After the heat treatment, the resulting powder was immersed in 1 M HCl for at least 2 h to remove magnesium oxide and 1 wt% hydrofluoric acid for at least 2 h to remove SiO_X that was possibly formed during the synthesis. The material was then vacuum-filtered and dried at 60 ^{o}C in the oven overnight. The as-synthesized silicon/carbon composite material was kept in a vial for future use.

Bulk Si

The Si metal powder was ball-milled with planetary ball mill at 400rpm for 12 hr. Agate jar and milling media were used and the ball-to-powder weight ratio was approximately 10:1.

Air-oxidation of Mg_2Si

The same conditions as CO-OP were used for air-oxidation of Mg_2Si, except that instead of flowing CO_2, both ends of the tube furnace were open to ambient condition in order to introduction of air during heat treatment. After the heat treatment, acid leaching was performed to remove MgO from the sample and obtained porous Si for electrochemical performance testing.

Materials Characterization

X-ray diffractometers (Rigaku SmartLab (40kV, 44mA) and Rigaku Miniflex 600 (40kV 25mA)) were used to investigate the crystal structures and composition of the samples. The powder morphology was characterized using a field emission scanning electron microscope (FEI Quanta 200F) and transmission electron microscope (FEI Technai G2 20 Twin with 200kV LaB_6 electron source). The carbon content of the carbon-coated porous Si composite was tested from thermogravimetric analysis/differential scanning calorimetry (TA Instrument SDT Q600) performed up to an approximate temperature range from 25 °C to 700 °C at a heating rate of 10 °C/min under air flow. Energy dispersive spectroscopy (Tescan Vega3) was used to perform elemental analysis. Raman spectroscopy (Horiba LabRAM HR system equipped with 532 nm laser) was used to investigate carbon in the sample. In situ high temperature XRD results were collected using the aforementioned Rigaku SmartLab equipped with an Anton Paar XRK900S in-situ high temperature chamber. The XRD data were continuously collected during heating and cooling. Each full scan took approximately 30 min and the scan range (2θ) was from 25^{o} to 45^{o}, in which all the main peaks of Si, Mg_2Si, and MgO are found. X-ray nano-computed tomography (Zeiss, Xradia Ultra 810) was used to analyze the internal microstructures.

Electrochemical Measurements

To evaluate the electrochemical properties of the carbon-coated macroporous Si, CR2032-type coin cells, consisting of the as-synthesized silicon/carbon composite as a working electrode and lithium metal chip (MTI) as the counter electrode, were assembled in an argon-filled glove box, in which the moisture and oxygen levels were regulated below 0.5 ppm. The working electrodes were prepared by slurry-casting (or doctor-blading), whereby the slurry composed of silicon/carbon active material (60 wt%), Super P45 carbon black conducting agent (20wt%), and poly(acrylic acid) (PAA, average molecular weight of 100kg/mol, Sigma–Aldrich) / sodium carboxymethyl cellulose (CMC, 5wt% in high purity water, Sigma–Aldrich) binder (20 wt%, PAA/CMC=1:1 by weight) in purified deionized water, was evenly spread onto copper foil (current collector) and vacuum-dried at 155 ^{o}C for 2 h to remove water and densify the electrode

structure. The electrolyte used was 1.3M lithium hexafluorophosphate ($LiPF_6$) in ethylene carbonate (EC)/diethylene carbonate (DEC) (3:7 by volume) with 10 wt% fluoroethylene carbonate (FEC) additive. Cycling performance was measured using a Neware (BTS 4008) and/or Arbin battery cycler (BT2000 model) at various C-rates; 0.05 C for the first cycle (1 C was calculated based on 2000 mAh/g of active material) and after the first cycle, all other C-rates were re-calculated based on the first lithiation capacities of each coin cell. The voltage range for the galvanostatic cycling was 0.01–1.2 V. Monolayer polypropylene membrane (Celgard 2400) was used as a separator.

1. B. Metz, O. Davidson, H. d. Coninck, M. Loos and L. Meyer, *IPCC special report on carbon dioxide capture and storage*, Cambridge University Press, New York, NY (United States); Intergovernmental Panel on Climate Change, Geneva (Switzerland). Working Group III, 2005.
2. C. Stewart and M.-A. Hessami, *Energy Conversion and Management*, 2005, 46, 403-420.
3. J. Yu, J. Low, W. Xiao, P. Zhou and M. Jaroniec, *Journal of the American Chemical Society*, 2014, 136, 8839-8842.
4. G. Yin, M. Nishikawa, Y. Nosaka, N. Srinivasan, D. Atarashi, E. Sakai and M. Miyauchi, *ACS Nano*, 2015, 9, 2111-2119.
5. S. N. Habisreutinger, L. Schmidt-Mende and J. K. Stolarczyk, *Angewandte Chemie International Edition*, 2013, 52, 7372-7408.
6. A. Goeppert, M. Czaun, J.-P. Jones, G. K. Surya Prakash and G. A. Olah, *Chemical Society Reviews*, 2014, 43, 7995-8048.
7. C. Maeda, Y. Miyazaki and T. Ema, *Catalysis Science & Technology*, 2014, 4, 1482-1497.
8. W.-L. Dai, S.-L. Luo, S.-F. Yin and C.-T. Au, *Applied Catalysis A: General*, 2009, 366, 2-12.
9. A. Chakrabarti, J. Lu, J. C. Skrabutenas, T. Xu, Z. Xiao, J. A. Maguire and N. S. Hosmane, *Journal of Materials Chemistry*, 2011, 21, 9491-9493.
10. Z. Xing, X. Luo, Y. Qi, W. F. Stickle, K. Amine, J. Lu and X. Ji, *ChemNanoMat*, 2016, 2, 692-697.
11. Z. Xing, B. Wang, W. Gao, C. Pan, J. K. Halsted, E. S. Chong, J. Lu, X. Wang, W. Luo, C.-H. Chang, Y. Wen, S. Ma, K. Amine and X. Ji, *Nano Energy*, 2015, 11, 600-610.
12. M. S. Chandrasekharaiah, J. L. Margrave and P. A. G. O'Hare, *Journal of Physical and Chemical Reference Data*, 1993, 22, 1459-1468.
13. W. K. Chu, S. S. Lau, J. W. Mayer, H. Müller and K. N. Tu, *Thin Solid Films*, 1975, 25, 393-402.
14. M. R. J. van Buuren, F. Voermans and H. vanKempen, *The Journal of Physical Chemistry*, 1995, 99, 9519-9522.
15. L. Stolt, O. Thomas and F. M. d'Heurle, *Journal of Applied Physics*, 1990, 68, 5133-5139.
16. X. Niu and L. Lu, *Advanced Performance Materials*, 1997, 4, 275-283.
17. J. Ahn, D.-H. Lee, M. S. Kang, K.-J. Lee, J.-K. Lee, Y.-E. Sung and W. C. Yoo, *Electrochimica Acta*, 2017, 245, 893-901.
18. B. E. Deal and A. S. Grove, *Journal of Applied Physics*, 1965, 36, 3770-3778.
19. J. Liang, X. Li, Z. Hou, C. Guo, Y. Zhu and Y. Qian, *Chemical Communications*, 2015, 51, 7230-7233.
20. B. Campbell, R. Ionescu, M. Tolchin, K. Ahmed, Z. Favors, K. N. Bozhilov, C. S. Ozkan and M. Ozkan, *Scientific Reports*, 2016, 6, 33050.
21. Z. Lu, N. Liu, H.-W. Lee, J. Zhao, W. Li, Y. Li and Y. Cui, *ACS Nano*, 2015, 9, 2540-2547.
22. R. Yi, F. Dai, M. L. Gordin, H. Sohn and D. Wang, *Advanced Energy Materials*, 2013, 3, 1507-1515.
23. Y.-S. Hu, R. Demir-Cakan, M.-M. Titirici, J.-O. Müller, R. Schlögl, M. Antonietti and J. Maier, *Angewandte Chemie International Edition*, 2008, 47, 1645-1649.
24. H. Jia, P. Gao, J. Yang, J. Wang, Y. Nuli and Z. Yang, *Advanced Energy Materials*, 2011, 1, 1036-1039.
25. H. Kim, B. Han, J. Choo and J. Cho, *Angewandte Chemie*, 2008, 120, 10305-10308.
26. N. Dimov, S. Kugino and M. Yoshio, *Electrochimica Acta*, 2003, 48, 1579-1587.

27. J.-I. Lee, J.-H. Park, S.-Y. Lee and S. Park, *Physical Chemistry Chemical Physics*, 2013, 15, 7045-7049.
28. S.-H. Ng, J. Wang, D. Wexler, K. Konstantinov, Z.-P. Guo and H.-K. Liu, *Angewandte Chemie International Edition*, 2006, 45, 6896-6899.
29. R. Huang, X. Fan, W. Shen and J. Zhu, *Applied Physics Letters*, 2009, 95, 133119.
30. S. H. Ng, J. Wang, D. Wexler, S. Y. Chew and H. K. Liu, *The Journal of Physical Chemistry C*, 2007, 111, 11131-11138.
31. Y. K. Rao, A. Adjorlolo and J. H. Haberman, *Carbon*, 1982, 20, 207-212.
32. J. Hunt, A. Ferrari, A. Lita, M. Crosswhite, B. Ashley and A. E. Stiegman, *The Journal of Physical Chemistry C*, 2013, 117, 26871-26880.
33. P. Lahijani, Z. A. Zainal, M. Mohammadi and A. R. Mohamed, *Renewable and Sustainable Energy Reviews*, 2015, 41, 615-632.
34. F. Meshkani and M. Rezaei, *Catalysis Communications*, 2011, 12, 1046-1050.
35. Y. Jiao, W. Tian, H. Chen, H. Shi, B. Yang, C. Li, Z. Shao, Z. Zhu and S.-D. Li, *Applied Energy*, 2015, 141, 200-208.
36. N. Bost, M. R. Ammar, M. L. Bouchetou and J. Poirier, *Journal of the European Ceramic Society*, 2016, 36, 2133-2142.
37. L. S. Schadler, S. C. Giannaris and P. M. Ajayan, *Applied Physics Letters*, 1998, 73, 3842-3844.
38. G. Song, X. Zhu, R. Chen, Q. Liao, Y.-D. Ding and L. Chen, *Chemical Engineering Journal*, 2016, 283, 175-183.